metals

MDPI

Article

Indentation of Commercial Pure Titanium Processed by Cold Rolling

Diaoyu Zhou [1,2,3,*], Jiasheng Yu [1], Yiwei Dong [1], Yalu Qin [1] and Xinwei Hao [1]

[1] Materials Science and Engineering, North University of China, Taiyuan 030051, China; yujiasheng@nuc.edu.cn (J.Y.); 15735348889@163.com (Y.D.); yaluqin@nuc.edu.cn (Y.Q.); 18935128059@163.com (X.H.)
[2] College of Materials Science and Engineering, Tianjin University, Tianjin 300354, China
[3] Zhejiang Honghe Medica Technology Company Limited, Jiaxing 314001, China
* Correspondence: zhoudiaoyu@nuc.edu.cn

Abstract: In this work, the effects of plastic deformation on the indentation behaviors of commercial pure titanium alloy were investigated. Titanium experienced various kinds of deformation by cold rolling processes, and the indentation behaviors were measured using microindentation. The results showed the most deformed sample experienced the largest indentation resistance and had the highest dislocation density and the indentation size influenced the indentation behavior of the CP-Ti. The effect of strain on Vickers hardness demonstrated the dominant role of the dislocation motion in the indentation deformation of CP-Ti alloy. The dependence of the indentation hardness on both the maximum indentation load and the indentation residual depth suggested there exists size effect in the indentation. The effect of the plastic strain on the energy ratio suggested the energy ratio is related to the microstructure in materials. Additionally, the linear relationship between the energy ratio on the indentation depth ratio was obtained for hcp-structured Titanium alloys.

Keywords: titanium; cold-rolled; plastic deformation; indentation; Vickers hardness

check for updates

Citation: Zhou, D.; Yu, J.; Dong, Y.; Qin, Y.; Hao, X. Indentation of Commercial Pure Titanium Processed by Cold Rolling. *Metals* **2024**, *14*, 327. https://doi.org/10.3390/met14030327

Academic Editor: Zbigniew Pater

Received: 18 January 2024
Revised: 21 February 2024
Accepted: 11 March 2024
Published: 13 March 2024

Copyright: © 2024 by the authors. Licensee MDPI, Basel, Switzerland. This article is an open access article distributed under the terms and conditions of the Creative Commons Attribution (CC BY) license (https://creativecommons.org/licenses/by/4.0/).

1. Introduction

It is well known that the severe plastic deformation method is commonly applied to improve the mechanical properties of metallic alloys by grain refining [1,2]. Severe plastic deformation can be achieved when a material can overcome plastic deformation repeatedly without a shape change, that is, the original shape at the beginning of the plastic deformation is the same as that in the end [3]. By repeating the process, the plastic strain of the material can be increased in effect after each cycle. There appear to be high dislocation densities and large internal strains in these severely deformed metals. Several studies have analyzed plasticity properties by changing the materials scale to fine grain sizes [4–8]. The severely deformed alloys have interesting and unique behaviors, including high strength with superplasticity and ductility because of their high internal strain, which is not usually observed in the conventional mildly deformation and coarse grained materials [9]. There are several methods to achieve severe plastic deformation, including accumulative rolling bonding (ARB), equal channel angular pressing (ECAP), repetitive corrugation and straightening (RCS), high pressure and torsion (HPT), etc. Among the existing various plastic deformation processes, traditional rolling has been found to be a controllable and easy technique to give alloys ultrafine structures in a large quantity with mass production because of its high rolling speed.

Titanium and titanium alloy is widely applied in automotive, aerospace, sports, the chemical industry, and other fields for the advantage of excellent strength, high-temperature resistance, low density, corrosion resistance, and other properties [10–13]. However, pure titanium alloy without deformation or heat-treated have limited applications because of its low strength. To enhance its comprehensive mechanical performance, cold rolling method

combined with heat treatment is applied to refine grain sizes of commercial pure titanium (CP-Ti) [14–16]. Sun et al. [17] investigated the impacts of the rolling reductions on the textures and microstructures evolutions of CP-Ti sheets and developed an accurate crystal plasticity finite element model to predict its rolling deformation behaviors. The results showed that the twins, including the extension twins and compression twins, and the slip become more likely contribute to the plastic deformations during the total rolling process. Chen et al. [18] fabricated the heterostructure for the commercial pure Ti sheets with an initial wavy profile combined with the rolled and annealed process, and observed that a bi-gradient microstructures—including gradient texture and gradient grain size—is built. In this, the mean grain size decreases but the split-basal texture becomes stronger from the trough zone to the crest zone. Lee et al. studied the anisotropy behaviors after the tensile deformation of the CP-Ti plate in the rolling (RD) and transverse direction (TD), by in situ SEM-EBSD measurement and stress-relaxation [19]. The results show that the strain-hardening behaviors of polycrystalline α-Ti appears the anisotropy due to the GB-mediated deformation and GB-dislocation interactions, which contribute to the particular orientation relationship between the grain pairs. Multi-pass cold rolling to varying thickness reductions was applied to fabricate the ultrafine-grained (UFG) Ti Grade 2 with the purpose of changing both of its microstructural characteristics, including grain size distribution, dislocation density and grain boundary features, as well as its textures, including the texture components and tensity [20]. This allowed for an analysis of the difference between the effects of microstructures and textural evolutions on the work hardening using the annealing effect for the cold-rolled titanium. It is a cost-effective and promising way to optimize the cold rolling process and improve its mechanical properties.

As a new testing method, indentation technology is widely applied to evaluate the local mechanical feature of samples, including metals, coatings, polymers, composites etc., at both micro and nano scales. This has gained increasing attention recently as a fast method that does not disrupt the materials structures and other properties [21]. Additionally, the indentation technique can probe a mechanical response to a very low applied load, and the behavior can be mechanically and physically analyzed [2]. The load-displacement curve obtained by microindentation experiment can not only obtain the relevant performance parameters of the elastic-plastic properties for the material quantitatively, but also reveal the microscopic deformation mechanism inside the material [22]. Yapici et al. [23] analyzed the anisotropic characters of material after ECAP and cold rolling processing and found that treatment caused stronger crystallographic texture. Li et al. [24] studied the mechanical property of the forged Ti-1023 material using microindentation experiments with different indentation loads and various loading speeds, and observed that the indentation Young's modulus nearly kept same and H decreased at higher load level. Ellard et al. [25] investigated the mechanical properties of the intermetallic Ti-48Al-2Nb-0.7Cr-0.3Si sheet by analyzing the united impacts of rapid cooling, hot-rolling, and heat treatment on the grain refinement and found that the indentation plastometry based on profilometry for the samples after the rolled and heat treated processing improved the mechanical properties' contrast with the as-cast and as-rolled specimen. Mahadule et al. [26] investigated the impact of plastic deformation on the crystallographic texture evolution for the Ti-15V-3Cr-3Sn-3Al (Ti-15333) alloy. With unidirectional cold rolling using the combined experimental and numerical methods, they observed that both the von Mises strain and the average von Mises stress values enlarged with the deformation increase. Arohi et al. [27] investigated the microstructures evolution and mechanical behaviors of metastable β Ti-5Al-5V-5Mo-3Cr alloys (ATI, Brackenridge, PA, USA)after the thermomechanical processing, and the results show that the distinct thermomechanical processing can improve its mechanical property with reduced rolling deformation. However, it is very difficult to connect the indentation feature with the plastic strain state induced in the plastic deformation history. Rolling can be easily determined by changing the thickness of the sample. As a result, the rolling process is very beneficial for evaluating the influence of plastic deformation history quantitatively on the relevant indentation feature of the samples [28].

Based on the above, the present article aimed to extensively research the impact of the history of plastic deformation on the indentation behaviors of the CP-Ti after cold-rolling using microindentation measurement methods. Additionally, the effects of the harness and energy dissipated on indentation load and strain are discussed. Some of the conclusions can also be used for all the crystalline ductile materials.

2. Experimental

2.1. Materials and Processing Methods

The commercially pure titanium (CP-Ti) sheets purchased from the Regal light metal company in Guangzhou, China were applied in present research, and the composition is given in Table 1. The original titanium sheet is the as-annealed state with equiaxed with an average grain size of 10 μm. The samples were obtained by cutting using diamond saw and prepared by the cold rolling technology. Figure 1 displays the cold rolling flow diagrams for the CP-Ti sheets in this work. Its original size is 50 mm × 50 mm × 5 mm. Prior to the cold rolling, all the CP-Ti sheets were pre-heated to 460 °C in a furnace in the air for half an hour. Then the heat-treated Ti sheets were cold-rolled quickly at a temperature of 200 °C for the two symmetrical machine rolls and the samples is in the center on a rolling machine (CX210, Corbeil Equipment Company Inc., Rochester, NY, USA). In this work, four different specimen thickness (D_t)—4.00, 3.00, 2.00, and 1.00 mm—were achieved by cold rolling with about 5% reduction per rolling pass, corresponding to the thickness reductions of 20%, 40%, 60%, and 80%, respectively. After cold rolling, all the CP-Ti samples with the size of 5 mm × 5 mm × D_t were obtained in the square shape for further experimental analysis. Concurrently, the original thickness sample (0% thickness reduction) without rolling was also prepared for comparison. After cold rolling, the ND–RD (Normal Direction–Rolling Direction) plane was taken for the microindentation analysis, as shown in Figure 1. All samples were mechanical polished using the SiC sandpaper starting from 100# to 2000#, followed by the final polish with colloidal silica suspension to mirror-like surface. They were then carefully cleaned with acetone, ethyl alcohol, and deionized water and dried by hair dryer for the subsequent microindentation tests.

Table 1. Composition of commercially pure titanium (wt.%).

C	Fe	H	N	O	Ti
0.08	0.3	0.0015	0.05	0.3	Bal.

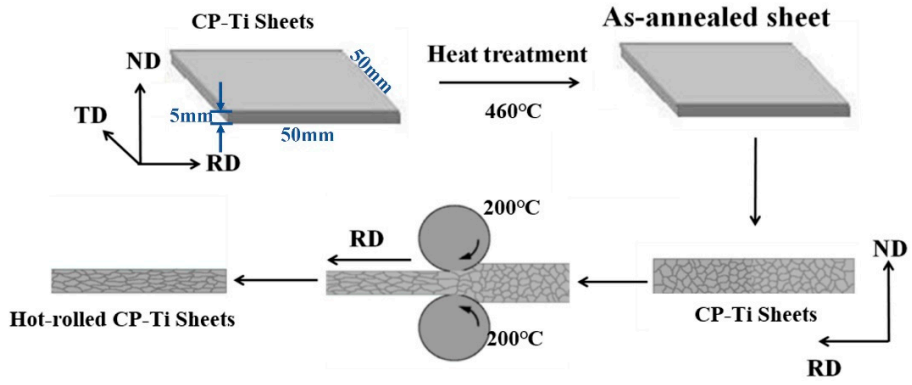


Figure 1. The rolling flow diagrams with specimen dimensions for the CP-Ti sheets.

2.2. Microindentation Tests

Microindentation tests were performed on the ND–RD plane mirror-like surface after polishing, which is parallel to the rolling direction for all the five cold-rolled specimens by using a Microhardness Tester (Hysitron TI 980 TriboIndenter, Bruker, Billerica, MA, USA). The diamond Vickers indenter (Mitutoyo, Sakado, Japan)was applied instead of spherical indenter in this work. Five different indentation loads of 100, 200, 300, 400, and

500 mN were used for each sample, and at least three indentations were repeated for each indentation load. The preload of 10 mN was applied to the indenter prior to the indentation to avoid the impact effect. Both the loading time and unloading time were 5 s, with an intermediate maintenance pause for 2 s for each indentation cycle.

3. Results and Discussion

3.1. Indentation Deformation of the Cold-Rolled CP-Ti

Figure 2 shows the original indentation load-displacement curves of the cold-rolled CP-Ti, with various maximum indentation loads for the sample with 60% thickness reduction. The indentation depth for both the maximum depth and the residual depth is the lowest under the maximum indentation load of 100 mN. The larger indentation load, as expected, the deeper indentation depth. It can also be seen that the five loading curves overlap with various indentation loads, which means the different loading rate has a negligible effect on the microindentation behavior for the cold-rolled CP-Ti under the various loading conditions. There exists a mild increase in unloading curve slope with the increasing of the maximum load, which can be explained by the elastoplastic recovery of sample. There exists strong interaction among the dislocations and the pile-up of dislocations in plastic deformation zones during the loading-unloading progress. During the unloading process, the mobile dislocations continuously move to other slip planes under the influence of plastic deformation. After reaching a certain state, these dislocations will combine with each other and annihilate, which can reduce strain energy and improve material stability. At the same time, dimensional deformation is also significantly reduced, which will have a certain impact on material properties [29].

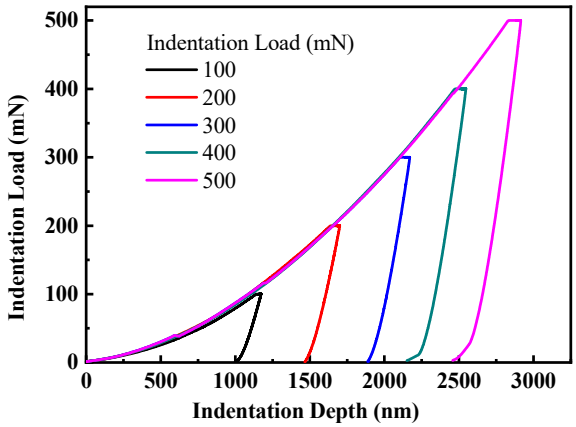


Figure 2. Typical indentation load-displacement curves of cold-rolled CP-Ti sheets under the different maximum indentation loads (thickness reduction = 60%).

Figure 3 exhibits the typical indentation loading-unloading curves of the cold-rolled CP-Ti sheets with different thickness reductions under the maximum load of 100 mN. It can be observed that the five samples with different thickness reductions have a similar indentation curve. The 0% thickness reduction specimen without rolling has the largest indentation depth, and the 80% thickness reduction one has the least indentation depth. The reason is that there appears to be strain hardening related to the plastic deformation of CP-Ti sheets in cold rolling process, which will be discussed later. The strain hardening enhanced with the increasing of the thickness reduction which is positive related to plastic deformation. With the increase of the thickness reduction for the CP-Ti sheets (TW Metals, Agawam, MA, USA), the dislocation density enhances, which can be attributed to the generation during the whole rolling process and its strong interactions between dislocations. This suggests that the specimen with maximum deformation (80%) experienced the largest resistance to indentation deformation and has the highest dislocation density. Conversely, the similar unloading curves from Figure 3 for all the different thickness reductions samples

demonstrate that the elastoplastic recovery is independent of its plastic deformation history under the same conditions.

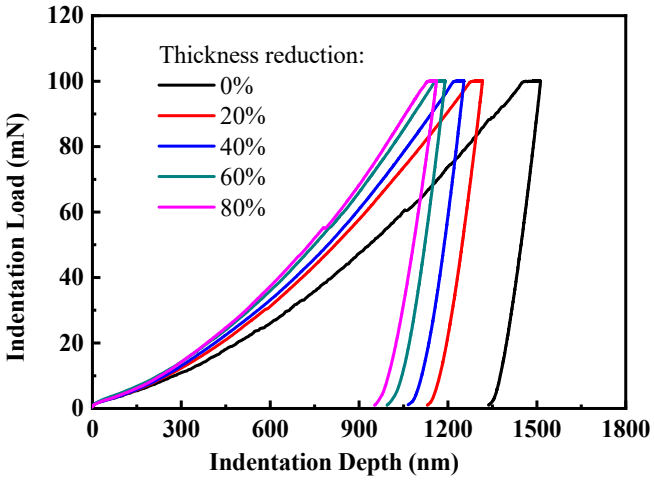


Figure 3. Typical indentation load-displacement curves of cold-rolled CP-Ti sheets with different thickness reductions (F_{max} = 100 mN).

Generally speaking, the relation between microindentation load and depth for a homogeneous material can be expressed as follows [30]

$$F = K_m {H_m}^n \text{ and } F = K_r {H_r}^m \quad (1)$$

where F represents indentation load, H_m and H_r are maximum indentation depth and residual indentation depth, respectively. K_m and K_r are a constant related to the material elastoplastic feature, and n is a constant index. From Figure 2, the maximum depth can be obtained for the corresponding maximum microindentation load. As a result, the relation of maximum microindentation depth and maximum indentation load for CP-Ti sheets can be obtained in Figure 4. As expected, the indentation displacement enlarged with the increase of the load. Otherwise, the more severe the plastic deformation (the larger thickness reduction), the shallower of the indentation depth, which is consistent with the results from Figure 3. Based on Equation (1) to curve-fit the data in Figure 3, the power index can be acquired, $n = 1/k \approx 1.8$, which is different from 1.5 for the microindentation results of CP-Ti treated via ECAP using the same diamond Vickers indenter [29]. This means there is a little surface microstructure difference between the cold-rolling and the ECAP process after plastic deformation for the same Ti sheets. The stress field created by ECAP generated lower stress concentration compared with the cold rolling method. The various values of K_m can also be obtained according to the intercept between the curve and $logF$ for all the cold-rolled CP-Ti samples. This is owing to the dislocation formation in all the cold worked materials and the increasing dislocation density with the enlarged amount of plastic degree for the deformed CP-Ti sheets. The strong interactions between the indenter and the dislocations can introduce higher resistance to prevent the movement of Vickers indenter in the severely deformed samples. As a result, the value of the constant K_m enlarged with the increasing of the thickness reduction for the cold-rolled CP-Ti sheets.

Similarly, Figure 5 exhibits the relation between the residual depth and the maximum microindentation load for CP-Ti sheets. The larger microindentation load, the more severe the plastic deformation and the deeper residual indentation depth, as expected. The cold-rolled CP-Ti samples of thickness reduction of 80% exhibits minimum residual depth, and those with 0% thickness have the largest residual depth under the same microindentation load, suggesting the influence of plastic deformation after cold rolling. The exponential indices, $m = 1/k \approx 1.8$, in Equation (1) can also be obtained, which represents the association of the indentation load and the residual indentation depth. Here, m is compatible with n for power relation. Both these two exponential indexes are less than 2, as obtained by

Chen et al. [29,31], suggesting that the microindentation size influences the indentation behaviors for the CP-Ti sheets. In particular, the reasons of indentation size effect are complex. The deviation of power index from 2 or the indentation size effect can be attributed to the influence of surface interaction, the blunting of the indenter tip, and the local residual stress gradient [32].

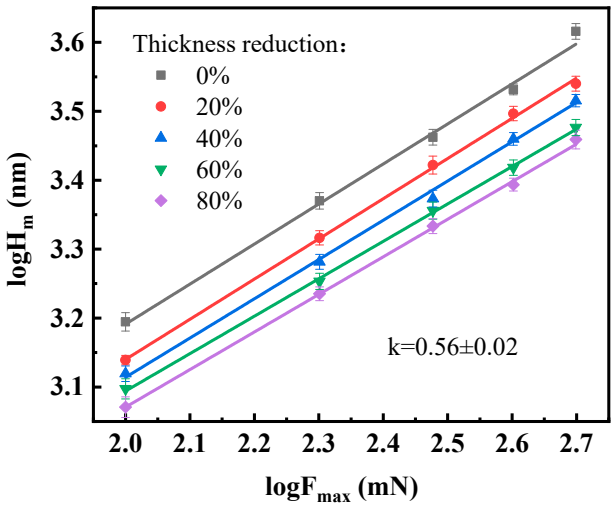


Figure 4. Dependence of maximum indentation depth on maximum microindentation load for the CP-Ti sheets.

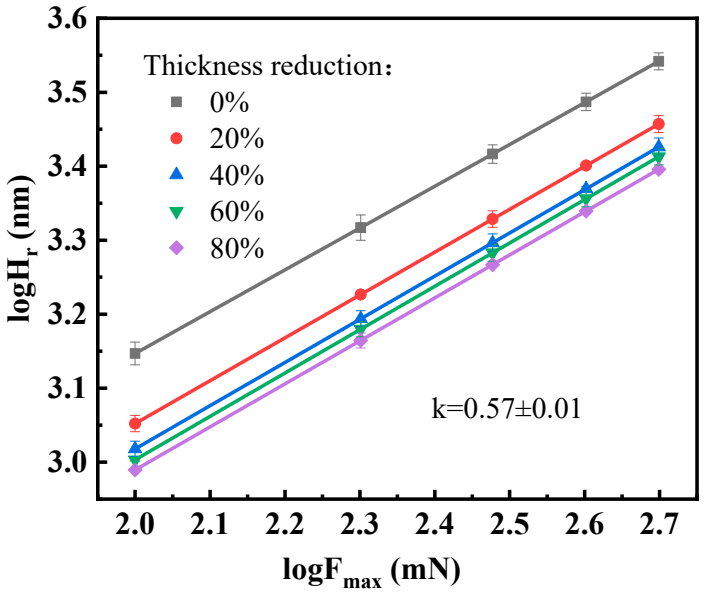


Figure 5. Dependence of residual indentation depth on maximum microindentation load for the CP-Ti sheets.

3.2. Vickers Hardness of the Cold-Rolled CP-Ti

Hardness is a powerful property for evaluating the deformation behavior of materials, and it serves as strong quality control for several processes, especially in the heat treatment of metals [33]. As is widely known, strain hardening is related to the dislocation multiplication after cold rolling, leading to the enhanced resistance to dislocation motion. From the previous work [34], the relationship between the Vickers hardness, H, and strain, ε_{eff}, can be expressed as

$$H = H_0 + 3\alpha\mu b\varepsilon_{eff}^n = H_0 + 3\alpha\mu b\left[-\ln(1-\tfrac{\Delta t}{t_0})\right]^n \quad (2)$$

where H_0 represents the Vicker hardness at $\varepsilon_{eff} = 0$, α corresponds to a constant, μ refers to the shear modulus, b refers to Burgers vector, t corresponds to the thickness of the cold-rolled CP-Ti plate, $\Delta t/t_0$ is the thickness reduction, and n equals the strain exponent. The ε_{eff} here represents the compressive plastic effective strain along the thickness reduction. The values of 0, 0.22, 0.51, 0.92, and 1.61 for the effective strain represent the thickness reduction of 0, 20%, 40%, 60%, and 80%, respectively.

Figure 6 exhibits the relation between the Vickers hardness and the effective strain for CP-Ti samples with indentation load of 200 mN. Using Equation (2) to fit the data in Figure 6, n = 0.5 can be obtained, which is the same value of dislocation movement mechanisms during the plastic deformation, confirming the dominant role of the dislocation motion in the indentation deformation for the cold-rolled CP-Ti sample.

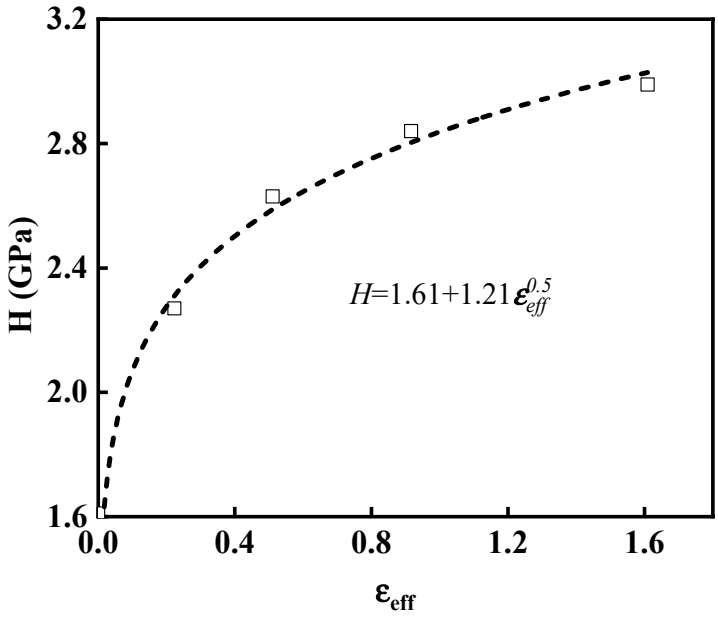


Figure 6. Dependence of the Vickers hardness on the effective strain for CP-Ti samples with the indentation load of 200 mN.

To explore the influence of the microindentation load on indentation Vickers hardness, which was defined as the microindentation load divided by the projected area of the indentation. Figure 6 shows the dependence of the average indentation Vickers hardness on the maximum microindentation load. It can be seen that the average Vickers hardness decreases with the increase of the microindentation load. The value of indentation Vickers hardness reduced drops slightly from 1.92 to 1.52 GPa for the specimen without cold rolling, with the maximum load in the range of 100 to 500 mN. A similar trend appeared for the other four cold-rolled samples, demonstrating the indentation size effect [35]. The curve-fitted spot lines in Figure 7 show the slope of the line representing the relationship exponential index between the average Vickers harness and indentation load, which ranges from 1.83 to the maximum value of 2.0. This is the same range as the results from Chen et al. [31], determining the close relation between the indentation Vickers hardness and indentation load for CP-Ti alloys.

Figure 8 displays the dependence of average Vickers hardness on the residual microindentation depth. With the increase of the residual microindentation depth, the average indentation Vickers hardness decreases slightly for all the cold-rolled CP-Ti sheets, indicating indentation size effect, which is as expected from the exponential index of m in Equation (1). Additionally, combined with the results from Figures 5 and 7, the cold-rolled CP-Ti sheets with 80% thickness reduction which owns the shallowest indentation depth exhibited maximum hardness, and the CP-Ti sheets for 0% thickness without cold-rolling has the smallest indentation hardness. This demonstrated that the average Vickers hardness

enhanced with the increase extent of plastic deformation due to the work hardening caused by dislocation motion.

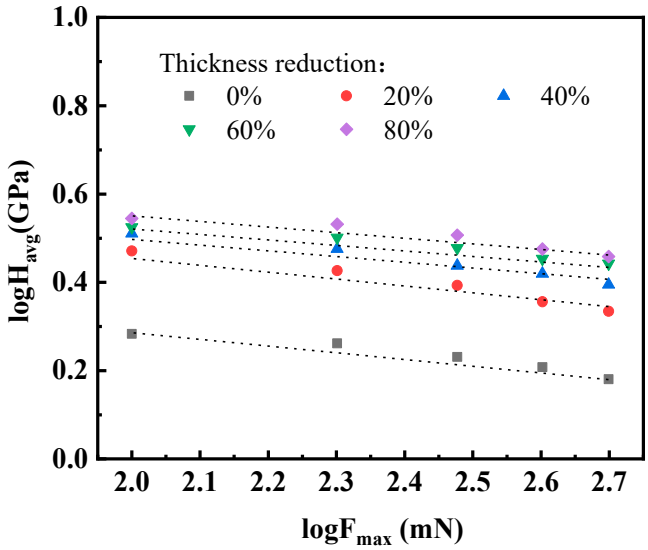


Figure 7. Dependence of the average indentation Vickers hardness on the maximum microindentation load.

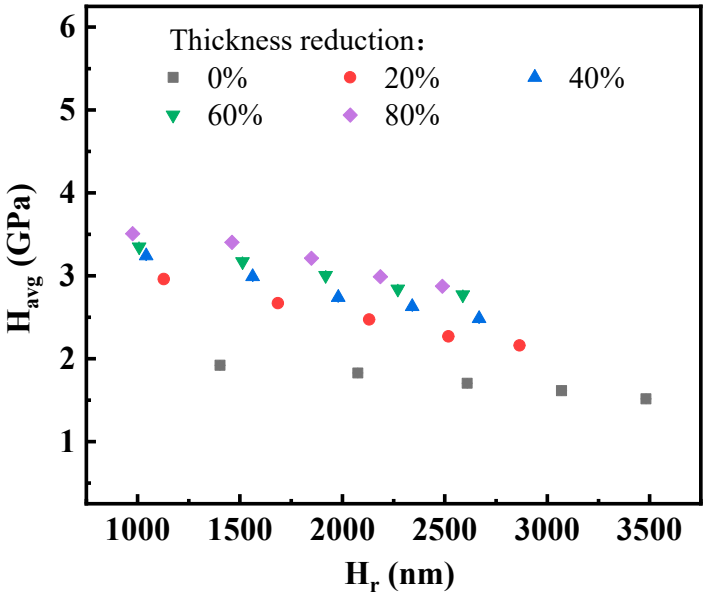


Figure 8. Relation of the average indentation hardness and the indentation residual depth.

3.3. Energy Dissipation of the Cold-Rolled CP-Ti

For the indentation loading-unloading curves, the plastic energy was determined by using the total energy ($E_{loading}$) stored and the elastic energy dissipated ($E_{unloading}$) in the sample as:

$$E_{plastic} = E_{loading} - E_{unloading} = \int_0^{\delta_{max}} Fd\delta - \int_{\delta_p}^{\delta_{max}} Fd\delta \quad (3)$$

Figure 9 shows the $E_{plastic}$ (plastic energy dissipated) in the indentation of all the cold-rolled CP-Ti samples with indentation load of 100 mN. It can be clearly observed that the plastic energy dissipated can be expressed as a nonlinear function of the thickness reduction after the cold-rolling treatment. The 0% thickness reduction specimen has the highest energy dissipation and maximum ductility, and the cold-rolled sample with

80% thickness reduction exhibits lowest energy dissipation. Such a result can be explained by the fact that greater thickness reduction causes the increased dislocation density during the plastic deformation processing. The larger the thickness reduction, the higher the dislocation density for the severe distorted CP-Ti sheets. The $E_{plastic}$ in the microindentation deformation of crystallized metals is a function of material microstructure, which should be addressed in the analysis.

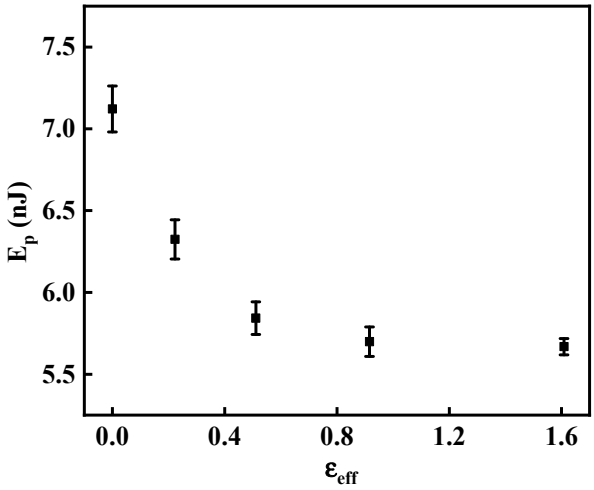


Figure 9. $E_{plastic}$ in the indentation with load of 100 mN.

To analyze the relationship between plastic energy dissipated and microindentation depth, Figure 10 displays the influence of residual indentation depth on plastic energy dissipated for different cold-rolled samples. Combined with Figure 9, the larger indentation residual depth, the higher plastic energy dissipated, the smaller effective strain (thickness reduction) for the CP-Ti sheets under the same indentation load. Through the data points fitting, a straight line with a slope, k, of 0.8127 is obtained, which suggests that the plastic energy dissipated is proportional to the third power of indentation residual depth.

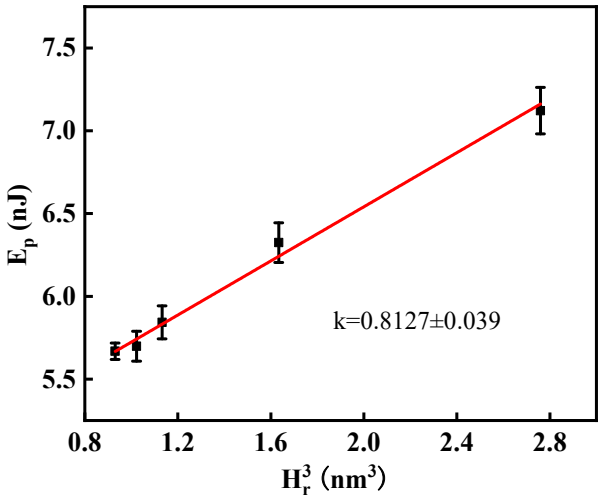


Figure 10. Plastic energy dissipated as a function of the residual depth with load of 100 mN for the different thickness reductions CP-Ti sheets.

The ratio of plastic energy dissipated to the total energy, $E_{plastic}/E_{total}$, can be determined via the typical indentation load-displacement curves. The effect of the plastic strain on the cold-rolled CP-Ti sheets on energy ratio can be seen in Figure 11. The error bars in the figure include the different results for various indentation loads. It can be seen that the energy ratio is independent with microindentation load for both the as-annealed

and cold-rolled Ti alloys, which is consistent with Malzender's work [36]. Obviously, the ratio is nonlinear relationship of the plastic strain after cold-rolling treatment, which is inversely related to the plastic strain. The 0% thickness reduction sample without cold rolling exhibits the maximum energy ratio. This can be explained by the higher dislocation density for the cold-rolled CP-Ti sheets after plastic deformation, which increases nominal hardness. The result indicated that the energy ratio is related to material microstructures. We should conduct in-depth research on this relationship and clarify its mechanism to provide support for improving the performance of materials, which is also one of the main research coldspots in this field.

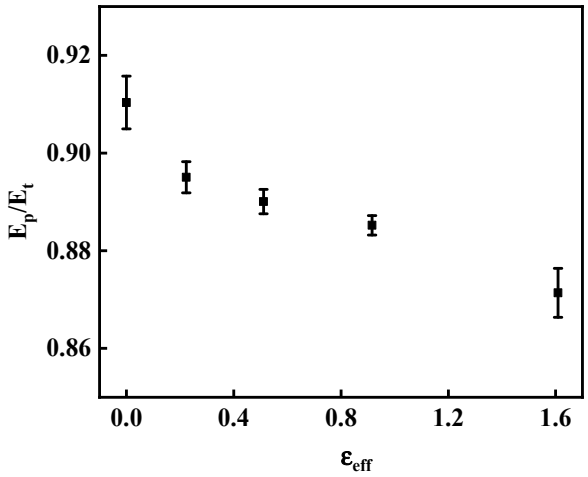


Figure 11. Effect of the plastic strain on the energy ratio for the different thickness reductions CP-Ti sheets.

Several works [36,37] have proposed a linear relationship between the microindentation energy ratio, $E_{plastic}/E_{total}$, and the microindentation depth retio, H_r/H_m, for $H_r/H_m > 0.4$. Figure 12 exhibits the variation of $E_{plastic}/E_{total}$, as a function of H_r/H_m, for different CP-Ti samples at the indentation load of 100 mN. The value of $E_{plastic}/E_{total}$ increase with the increase of H_r/H_m. The results indicated that the linear relation can also be used for hcp Titanium alloys materials (seen the dotted line in Figure 12), which is independent of the deformation history. Thus, a reasonable conclusion can be drawn that the linear association between the $E_{plastic}/E_{total}$ and H_r/H_m is suitable for all undeformed and deformed crystalline ductile materials.

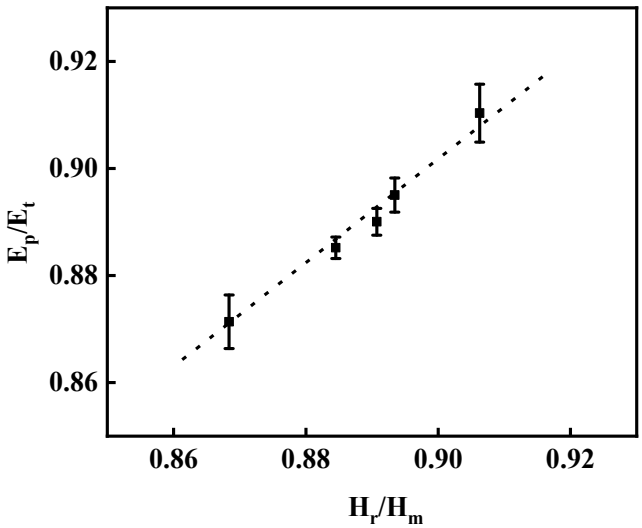


Figure 12. Effect of the indentation depth ratio, H_r/H_m, on the energy ratio, $E_{plastic}/E_{total}$, at the indentation load of 100 mN for the different thickness reductions CP-Ti sheets.

4. Conclusions

The commercial pure titanium alloys with various plastic deformations were fabricated using traditional cold rolling manufacturing process. The dependence of the indentation behaviors of cold-rolled CP-Ti on the plastic deformation was analyzed with different indentation load in this work. The original indentation load-displacement curves showed that the lager indentation load, the deeper indentation depth. The sample with maximum deformation experienced the largest indentation resistance and had the highest dislocation density. The exponential association between the microindentation load and the indentation depth suggested that indentation size influenced the indentation results of CP-Ti sheets. The effect of effective strain on Vickers hardness demonstrated the dominant role of dislocation motion in the indentation deformation of cold-rolled CP-Ti alloy. The average indentation Vickers hardness is negative related to both the maximum load and the indentation residual depth, suggesting there exists a size effect in indentation deformation process. The largest thickness reduction specimen exhibits maximum E_p, which suggested the energy dissipation in the deformation of crystallized metals is related to its microstructure. Additionally, the plastic energy dissipated is closely related to residual depth with slope of 0.8127. The influence of the plastic strain on the calculated E_p/E_t suggested the energy ratio is related to the microstructure in materials. Finally, the linear relationship between the energy ratio, E_p/E_t, and the indentation depth ratio, $H_r/H_{m,}$ was obtained for hcp structured Ti materials, which can also be applied to all undeformed and deformed hcp crystalline ductile materials in future discussion.

Author Contributions: Conceptualization, D.Z. and X.H.; Methodology, J.Y.; Software, Y.D.; Validation, J.Y., Y.D. and Y.Q.; Formal analysis, D.Z.; Investigation, J.Y.; Resources, Y.D.; Data curation, Y.Q.; Writing—original draft, D.Z.; Writing—review & editing, D.Z.; Visualization, X.H.; Supervision, D.Z.; Project administration, D.Z.; Funding acquisition, D.Z. All authors have read and agreed to the published version of the manuscript.

Funding: The research was sponsored by the Research Project Supported by Shanxi Scholarship Council of China (2023-145).

Data Availability Statement: The data presented in this study are available on request from the corresponding author (privacy).

Conflicts of Interest: Author Diaoyu Zhou was employed by the company Zhejiang Honghe Medica Technology Company Limited. The remaining authors declare that the re-search was conducted in the absence of any commercial or financial relationships that could be construed as a potential conflict of interest.

References

1. Zhang, J.; Liu, K.; Chen, T.; Xu, C.; Chen, C.; Yan, D.S.; Dippel, A.C.; Sun, J.; Ding, X.D. Inverse gradient nanostructure through gradient cold rolling demonstrated with superelasticity improvement in Ti-50.3Ni shape memory alloy. *J. Mater. Sci. Technol.* **2024**, *185*, 233–244. [CrossRef]
2. Hussain, G.; Shehbaz, T.; Alkahtani, M.; Khaliq, U.A.; Wei, H. Nanomechanical, mechanical and microstructural characterization of electron beam welded Al2219-T6 tempered aerospace grade alloy: A comprehensive study. *Heliyon* **2024**, *10*, e23835. [CrossRef]
3. Fattahi, M.; Hsu, C.-Y.; Ali, A.O.; Mahmoud, Z.H.; Dang, N.P.; Kianfar, E. Severe plastic deformation: Nanostructured materials, metal-based and polymer-based nanocomposites: A review. *Heliyon* **2023**, *9*, e22559. [CrossRef]
4. George, V.; Mohammadreza, Y. Review of Nanoindentation Size Effect: Experiments and Atomistic Simulation. *Crystals* **2017**, *7*, 321.
5. Bond, T.; Badmos, A.; Ahmed, R.A.; Obayemi, J.D.; Salifu, A.; Rahbar, N.; Soboyejo, W.O. Indentation size effects in aluminum and titanium alloys. *Mater. Sci. Eng. A* **2022**, *839*, 142542. [CrossRef]
6. Stegall, D.E.; Mamun, M.A.; Crawford, B.; Elmustafa, A. Indentation size effect in FCC metals: An examination of experimental techniques and the bilinear behavior. *J. Mater. Res.* **2012**, *27*, 1543–1552. [CrossRef]
7. Zong, Z.; Soboyejo, W. Indentation size effects in face centered cubic single crystal thin films. *Mater. Sci. Eng. A* **2005**, *404*, 281–290. [CrossRef]

8. Pharr, G.M.; Herbert, E.G.; Gao, Y. The Indentation Size Effect: A Critical Examination of Experimental Observations and Mechanistic Interpretations. *Annu. Rev. Mater. Res.* **2010**, *40*, 271–292. [CrossRef]
9. Hayes, J.; Keyte, R.; Prangnell, P. Effect of grain size on tensile behaviour of a submicron grained Al–3 wt-%Mg alloy produced by severe deformation. *Mater. Sci. Technol.* **2000**, *16*, 1259–1263. [CrossRef]
10. Zhang, Z.; Hosoda, S.; Kim, I.S.; Watanabe, Y. Grain refining performance for Al and Al–Si alloy casts by addition of equal-channel angular pressed Al–5 mass% Ti alloy. *Mater. Sci. Eng. A* **2006**, *425*, 55–63. [CrossRef]
11. Jun, T.S.; Sernicola, G.; Dunne, F.P.; Britton, T.B. Local deformation mechanisms of two-phase Ti alloy. *Mater. Sci. Eng. A* **2016**, *649*, 39–47. [CrossRef]
12. Jawed, S.F.; Rabadia, C.D.; Khan, M.A.; Khan, S.J. Effect of Alloying Elements on the Compressive Mechanical Properties of Biomedical Titanium Alloys: A Systematic Review. *ACS Omega* **2022**, *7*, 29526–29542. [CrossRef]
13. Meng, Q.; Bai, C.; Xu, D. Flow behavior and processing map for hot deformation of ATI425 titanium alloy. *J. Mater. Sci. Technol.* **2018**, *34*, 105–114. [CrossRef]
14. Cao, F.; Liu, R.; Kong, S.; Guo, N.; Xu, P.; Xu, G. Microstructural evolution, high temperature tensile deformation behavior, and deformation mechanism in an Mg–Zn–Y–Ca–Zr alloy processed by multidirectional forging and hot rolling. *J. Mater. Res. Technol.* **2023**, *27*, 6729–6743. [CrossRef]
15. Thakur, S.K.; Harish, L.; Das, A.K.; Rath, S.; Jha, B.K. Hot deformation behavior and processing map of Nb-V-Ti micro-alloyed steel. *Mater. Today Proc.* **2020**, *28*, 1973–1979. [CrossRef]
16. Li, B.; He, W.; Chen, Z.; Huang, H.; Liu, Q. Evolution of interface and collaborative deformation between Ti and steel during hot roll bonding. *Mater. Charact.* **2020**, *164*, 110354. [CrossRef]
17. Sun, Y.; Yang, X.; Liu, X.; Qiang, M.; Yue, X.; Chen, W. Analysis of Microstructure, Texture Evolution, and the Mechanism of Grain Refinement of Commercially Pure Titanium During Cold Rolling: Experiment and Simulation. *Adv. Eng. Mater.* **2023**. [CrossRef]
18. Chen, W.; Liu, G.; Gao, Y.; He, W.; Chen, Z.; Jiang, B. Fabrication of dual-gradient microstructure and their effects on the mechanical properties of commercial pure Ti. *J. Mater. Res. Technol.* **2023**, *24*, 3309–3322. [CrossRef]
19. Lee, M.-S.; Lee, J.-R.; Jeon, J.B.; Won, J.W.; Hyun, Y.-T.; Jun, T.-S. In-situ study of anisotropic strain-hardening and grain boundary mediated deformation in commercially pure titanium. *J. Mater. Res. Technol.* **2023**, *24*, 5389–5403. [CrossRef]
20. Majchrowicz, K.; Sotniczuk, A.; Adamczyk-Cieślak, B.; Chromiński, W.; Jóźwik, P.; Pakieła, Z.; Garbacz, H. The influence of microstructure and texture on the hardening by annealing effect in cold-rolled titanium. *J. Alloys Compd.* **2023**, *948*, 169791. [CrossRef]
21. Behera, A.; Gupta, R.; Yasin, G.; Nguyen, T.A.; Al, E. Mechanical and Tribological Properties Evaluation of Plasma-Sprayed Shape Memory Alloy Coating. *J. Alloys Compd.* **2021**, *863*, 158599.
22. Rominiyi, A.; Mashinini, P.M. Nanoindentation study of mechanical and wear properties of spark plasma sintered Ti-6Ni-xTiCN composites. *Ceram. Int.* **2023**, *49*, 2194–2203. [CrossRef]
23. Yapici, G.G.; Karaman, I.; Maier, H.J. Mechanical flow anisotropy in severely deformed pure titanium. *Mater. Sci. Eng. A* **2006**, *434*, 294–302. [CrossRef]
24. Jiang, L.; Guo, L.F.; Kai, M.X.; Jie, Z.M.; Wei, Y.Z. Micromechanical Study of the Forged Ti-1023 Titanium Alloy by Micro-Indentation. *Key Eng. Mater.* **2018**, *765*, 160–165.
25. Ellard, J.J.M.; Mathabathe, M.N.; Siyasiya, C.; Bolokang, A.S. Vacuum melting of compressed powders and hot rolling of the as-cast Ti-48Al-2Nb-0.7Cr-0.3Si intermetallic alloy: Mechanical properties and microstructural analysis. *J. Manuf. Process.* **2023**, *101*, 1214–1223. [CrossRef]
26. Mahadule, D.; Demiral, M.; Mulki, H.; Khatirkar, R.K. Experiments and Crystal Plasticity Finite Element Simulations of Texture Development during Cold Rolling in a Ti-15V-3Cr-3Sn-3Al Alloy. *Crystals* **2023**, *13*, 137. [CrossRef]
27. Arohi, A.C.; Shekhar, S.; Sen, I. Effect of thermomechanical processing on microstructure evolution and mechanical properties of metastable β Ti–5Al–5V–5Mo–3Cr alloy. *Mater. Chem. Phys.* **2024**, *314*, 128809. [CrossRef]
28. Yang, F.; Du, W.; Okazaki, K. Effect of cold rolling on the indentation deformation of AA6061 aluminum alloy. *J. Mater. Res.* **2011**, *20*, 1172–1179. [CrossRef]
29. Chen, R.; Yang, F.; Okazaki, K.; Imam, M.A.; Feng, C.R.; Pao, P. Indentation of titanium processed by equal channel angular pressing. *J. Phys. D Appl. Phys.* **2008**, *41*, 105407. [CrossRef]
30. Yang, F.; Peng, L.; Okazaki, K. Microindentation of aluminum. *Metall. Mater. Trans. A* **2004**, *35*, 3323–3328. [CrossRef]
31. Chen, R.; Yang, F.; Imam, M.A.; Feng, C.R.; Pao, P. Microindentation of titanium: Dependence of plastic energy on the indentation depth and time-dependent plastic deformation. *J. Mater. Res.* **2011**, *23*, 1068–1075. [CrossRef]
32. Alcalá, J.; Pike, L.M.; Giovannoni, J.J. Identification of Plastome Variants useful for Cytoplasmic Selection and Cultivar Identification in Onion. *J. Am. Soc. Hortic. Sci.* **1999**, *124*, 122–127. [CrossRef]
33. Pintaude, G. Hardness as an indicator of material strength: A critical review. *Crit. Rev. Solid State Mater. Sci.* **2023**, *48*, 623–641. [CrossRef]
34. Zhou, D.; Du, W.; Wen, X.; Qiao, J.; Liang, W.; Yang, F. Local Deformation and Texture of Cold-Rolled AA6061 Aluminum Alloy. *Materials* **2018**, *11*, 1866. [CrossRef] [PubMed]
35. Pugno, N.M. A general shape/size-effect law for nanoindentation. *Acta Mater.* **2007**, *55*, 1947–1953. [CrossRef]

36. Mencik, J.; Swain, M.V. Micro-indentation Test with Pointed Indenters. *Metals Forum* **1994**, *18*, 277–288.
37. Cheng, Y.; Cheng, C. Scaling, Dimensional Analysis, and Indentation Measurements. *Mater. Sci. Eng. R* **2004**, *44*, 91–149. [CrossRef]

Disclaimer/Publisher's Note: The statements, opinions and data contained in all publications are solely those of the individual author(s) and contributor(s) and not of MDPI and/or the editor(s). MDPI and/or the editor(s) disclaim responsibility for any injury to people or property resulting from any ideas, methods, instructions or products referred to in the content.